Comput Geosci
DOI 10.1007/s10596-013-9387-6

ORIGINAL PAPER

A monotone nonlinear finite volume method for diffusion equations and multiphase flows

Kirill Nikitin · Kirill Terekhov · Yuri Vassilevski

Received: 5 March 2013 / Accepted: 14 November 2013

Abstract We present a new nonlinear monotone finite volume method for diffusion equation and its application to two-phase flow model. We consider full anisotropic discontinuous diffusion or permeability tensors on conformal polyhedral meshes. The approximation of the diffusive flux uses the nonlinear two-point stencil which provides the conventional seven-point stencil for the discrete diffusion operator on cubic meshes. We show that the quality of the discrete flux in a reservoir simulator has great effect on the front behavior and the water breakthrough time. We compare two two-point flux approximations (TPFA), the proposed nonlinear TPFA and the conventional linear TPFA, and multipoint flux approximation (MPFA). The new nonlinear scheme has a number of important advantages over the traditional linear discretizations. Compared to the linear TPFA, the nonlinear TPFA demonstrates low sensitivity to grid distortions and provides appropriate approximation in case of full anisotropic permeability tensor. For nonorthogonal grids or full anisotropic permeability tensors, the conventional linear TPFA provides no approximation, while the nonlinear flux is still first-order accurate. The computational work for the new method is higher than the one for the conventional TPFA, yet it is rather competitive. Compared to MPFA, the new scheme provides sparser algebraic systems and thus is less computational expensive. Moreover, it is monotone which means that the discrete solution preserves the nonnegativity of the differential solution.

Keywords Numerical methods · Multiphase flows · Nonlinear scheme · Monotone discretization

This work has been supported in part by RFBR grants 11-01-00971, 12-01-31275, 12-01-33084, Russian Presidential grant MK-7159.2013.1, Federal target programs "Scientific and scientific-pedagogical personnel of innovative Russia" and "Research and development for priority directions of science and technology complex of Russia", ExxonMobil Upstream Research Company, and project "Breakthrough" of Rosatom

K. Nikitin (✉) · K. Terekhov · Y. Vassilevski
Institute of Numerical Mathematics, Russian Academy of Sciences, Moscow, Russia
e-mail: nikitin.kira@gmail.com

K. Nikitin · K. Terekhov
Nuclear Safety Institute, Russian Academy of Sciences, Moscow, Russia

K. Terekhov
e-mail: kirill.terehov@gmail.com

Y. Vassilevski
Moscow Institute of Physics and Technology, Dolgoprudny, Russia
e-mail: yuri.vassilevski@gmail.com

1 Introduction

Applications in reservoir simulation use different types of meshes such as tetrahedral, hexahedral, prismatic, octree, etc. All of them fall in the class of conformal meshes with polyhedral cells. The demand from the engineering community for a simple and accurate conservative method applicable to general conformal meshes and full anisotropic tensor permeability coefficients is very distinct.

The conservative linear methods on unstructured polyhedral meshes are well known: cell-centered finite volume (FV) with multipoint flux approximation (MPFA) [1], the KR mixed finite element (MFE) [3, 7], and the mimetic finite difference (MFD) [11] methods. They are second-order accurate and are not monotone even when the diffusion coefficient is moderately (1:100) anisotropic. The FV method with a linear two-point flux approximations (TPFA) is monotone but may be not even first-order accurate for

Published online: 13 December 2013

anisotropic problems or unstructured meshes. Nevertheless, this method is conventional in modeling flows in porous media due to its technological simplicity and monotonicity.

In this paper, we present a new cell-centered FV method that preserves solution positivity and discuss its application for multiphase flows. The method belongs to the class of methods with nonlinear flux discretizations [5, 6, 8, 12–14, 16, 20, 23]. The method is applicable to the 3D conformal polyhedral meshes and diffusion equations with heterogeneous full diffusion tensor [5] or advection–diffusion equations [14, 16]. The approximation of advective fluxes is based on the upwinding approach along with a piecewise linear reconstruction of the FV solution and a slope-limiting technique. In all cases of model equations, the method is exact for linear and piecewise linear solutions and thus one can expect the second-order truncation error. We note that in this paper, we consider the method that preserves nonnegativity of the discrete solution but still can violate the discrete maximum principle (DMP) [5]. However, the method can be modified [15] so that it provides the DMP and preserves the minimal compact stencil of the FV discretization. Other FV methods providing the DMP for the diffusion equation are proposed in [9, 10, 21].

The new nonlinear TPFA has a number of important advantages over the conventional linear TPFA. First, it demonstrates very low sensitivity to grid distortions. Second, it provides appropriate approximations in the case of full anisotropic permeability (diffusion) tensor. Third, being combined with the cell-centered FV method, it preserves solution positivity and thus provides a monotone discretization.

The TPFA schemes are technologically appealing due to the compact stencil of the FV discretization even on polygonal or polyhedral meshes. For cubic meshes, this stencil reduces to the conventional seven-point finite difference stencil. Compared to MPFA [1] scheme, the new scheme provides sparser algebraic systems and thus is less computational expensive. Moreover, it is monotone that means that the discrete solution preserves the nonnegativity of the differential solution.

The major computational overhead of the solution of the linear diffusion equation by the nonlinear FV method is related to two nested iterations in the nonlinear solver. The outer iteration is any linearization method, for instance, Picard method which guarantees solution positivity on each iteration. The inner iteration is the Krylov subspace method for solving linearized problems.

We consider applications of the new FV method to the solution of the two-phase flow equations [17]. The two-phase flow model concerns the secondary stage of oil recovery which is called water flooding. At this stage, water is injected into injection wells while oil is produced through production wells. We simulate the two-phase flow of immiscible fluids using the implicit pressure–explicit saturation (IMPES) and fully implicit methods. The IMPES method presumes the discretization and nested iteration solution of the diffusion equation for pressure. The implicit method presumes the straightforward discretization of the system of flow equations and the solution by Newton method that is nested iteration as well. We show that the quality of the discrete flux in a reservoir simulator has a great effect on the front behavior and the water breakthrough time. We compare two methods of the discrete flux definition: the conventional linear TPFA and the new nonlinear TPFA.

We emphasize that in special cases of orthogonal grid with isotropic or grid-aligned anisotropic permeability tensor (so-called $\mathbb{K}$-orthogonal grid) MPFA, linear TPFA and nonlinear TPFA are identical. On the other hand, if the grid is not $\mathbb{K}$-orthogonal, the linear TPFA provides no approximation of the flux, while the nonlinear TPFA is still first-order accurate and preserves the sparsity of the linear TPFA, in contrast to MPFA. Numerical experiments with the two-phase flow model demonstrate significant loss of accuracy due to the conventional TPFA or slow down of the simulation with MPFA and thus justify the use of the nonlinear TPFA alternative.

The paper outline is as follows. In the first section, we introduce the FV method and different approaches for the diffusive flux discretization. In the second section, we recall the two-phase flow model formulation and present two time discretization schemes: IMPES and fully implicit method. In the third section, we present the numerical results for the multiphase flows modeling using the conventional linear TPFA, MPFA, and new nonlinear TPFA schemes.

2 Finite volume method

Let Ω be a three-dimensional polyhedral domain with boundary consisting of two parts: $\Gamma = \Gamma_N \cup \bar{\Gamma}_D$ and $\Gamma_D \cap \Gamma_N = \emptyset$.

We consider a model steady diffusion problem for a conservative unknown c:

$$\begin{aligned} -\mathrm{div}(\mathbb{K}\nabla c) &= g \quad \text{in} \quad \Omega, \\ c &= g_D \quad \text{on} \quad \Gamma_D, \\ -(\mathbb{K}\nabla c)\cdot \mathbf{n} &= g_N \quad \text{on} \quad \Gamma_N, \end{aligned} \tag{1}$$

where $\mathbb{K}(\mathbf{x}) = \mathbb{K}^T(\mathbf{x}) > 0$ is a symmetric positive definite discontinuous (possibly anisotropic) full diffusion tensor, g is a source term, and $\mathbf{n}$ is the exterior normal vector.

Let $\mathcal{T}$ be a conformal polyhedral mesh composed of $N_{\mathcal{T}}$ shape-regular cells with planar faces. We assume that each cell T is a star-shaped 3D domain with respect to its barycenter $\mathbf{x}_T$, and each face f is a star-shaped 2D domain with respect to face's barycenter $\mathbf{x}_f$. We also assume that

$\mathcal{T}$ is face-connected, i.e., it cannot be split into two meshes having no common faces.

Let $\mathbf{q} = -\mathbb{K}\nabla c$ denote the diffusive flux. In general terms, the flux $\mathbf{q}$ of the conservative unknown c satisfies the mass conservation equation with a source term g:

$$\operatorname{div} \mathbf{q} = g \quad \text{in} \quad \Omega. \tag{2}$$

We derive cell-centered FV scheme with TPFA. Integrating Eq. 2 over a polyhedron T and using Green's formula, we get:

$$\int_{\partial T} \mathbf{q} \cdot \mathbf{n}_T \, \mathrm{d}s = \int_T g \, \mathrm{d}x, \tag{3}$$

where $\mathbf{n}_T$ denotes the outer unit normal to ∂T. Let f denote a face of cell T and $\mathbf{n}_f$ be the corresponding normal vector. For a single cell T, we always assume that $\mathbf{n}_f$ is the outward normal vector. In all other cases, we specify orientation of $\mathbf{n}_f$. It will be convenient to assume that $|\mathbf{n}_f| = |f|$ where $|f|$ denotes the area of face f. The Eq. 3 becomes

$$\sum_{f \in \partial T} \mathbf{q}_f \cdot \mathbf{n}_f = \int_T g \, \mathrm{d}x, \tag{4}$$

where $\mathbf{q}_f$ is the average flux density for face f.

For each cell T, we assign one degree of freedom, C_T, for the conservative unknown c. For simplicity, we shall refer to c as concentration. Let C be the vector of all discrete concentrations. If two cells T_+ and T_- have a common face f, our flux approximation with the two-point support, or the two-point flux approximation, is as follows:

$$\mathbf{q}_f^h \cdot \mathbf{n}_f = D^+ C_{T_+} - D^- C_{T_-}, \tag{5}$$

where D^+ and D^- are some coefficients. In the *linear* TPFA, these coefficients are equal and fixed. In the *nonlinear* TPFA, they may be different and depend on concentrations in surrounding cells. On face $f \in \Gamma_D$, the flux has a form similar to Eq. 5 with an explicit value for one of the concentrations. For the Dirichlet boundary value problem, $\Gamma_D = \partial\Omega$, substituting Eq. 5 into Eq. 4, we obtain a system of $N_{\mathcal{T}}$ equations with $N_{\mathcal{T}}$ unknowns C_T. The cornerstone of the cell-centered FV method is the definition of discrete flux (5).

2.1 Linear flux discretization

We consider an anisotropic diffusion tensor and a $\mathbb{K}$-nonorthogonal grid: neither co-normal vector $\mathbb{K}\mathbf{n}_f$, nor the vector $\mathbf{t}_f$ connecting collocation points $\mathbf{x}_-, \mathbf{x}_+$ are orthogonal to face f (Fig. 1).

For the flux through the interior face f, we have:

$$\mathbb{K}\nabla c \cdot \mathbf{n}_f = \nabla c \cdot (\mathbb{K}\mathbf{n}_f). \tag{6}$$

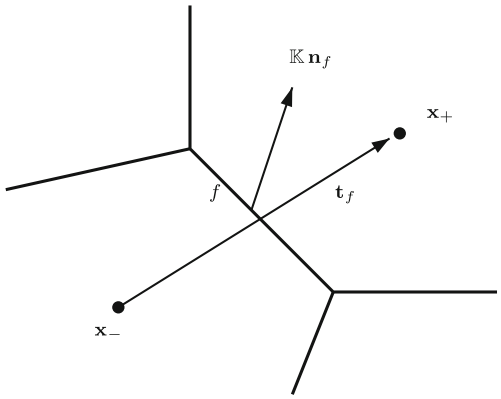

Fig. 1 Notations for the linear flux discretization

The linear TPFA of the $\mathbf{t}_f$-component of the concentration gradient is:

$$(\nabla c)^h_{\mathbf{t}} = \frac{C_+ - C_-}{|\mathbf{t}_f|}, \tag{7}$$

where $C_\pm = c(\mathbf{x}_\pm)$.

Replacing $\nabla c \cdot (\mathbb{K}\mathbf{n}_f)$ with $(\nabla c)^h_{\mathbf{t}} \, (\mathbb{K}\mathbf{n}_f) \cdot \frac{\mathbf{t}_f}{|\mathbf{t}_f|}$ and substituting Eq. 7 into Eq. 6, we get

$$\begin{aligned}(\mathbb{K}\nabla c)^h_f \cdot \mathbf{n}_f &= \frac{C_+ - C_-}{|\mathbf{t}_f|} \, \mathbb{K}\mathbf{n}_f \cdot \frac{\mathbf{t}_f}{|\mathbf{t}_f|} \\ &= \frac{\mathbb{K}\mathbf{n}_f \cdot \mathbf{t}_f}{|\mathbf{t}_f|^2} \, (C_+ - C_-) = \mathbb{T} \, (C_+ - C_-)\end{aligned} \tag{8}$$

with the transmissibility $\mathbb{T} = \dfrac{\mathbb{K}\mathbf{n}_f \cdot \mathbf{t}_f}{|\mathbf{t}_f|^2}$.

The flux through the boundary face is defined by the Dirichlet or Neumann data.

In case of $\mathbb{K}$-orthogonal mesh, $\mathbb{K}\mathbf{n}_f$ and $\mathbf{t}_f$ are colinear, and the expression (8) takes the form of the central finite difference and approximates the flux with at least first-order accuracy. In general case, the linear scheme may not provide approximation at all.

2.2 Nonlinear flux discretization

Let $\mathcal{F}_I$, $\mathcal{F}_B$ be the disjoint sets of interior and boundary faces, respectively. The subset $\mathcal{F}_J$ of $\mathcal{F}_I$ collects faces with jumping diffusion tensor. The sets $\mathcal{F}_T$ and $\mathcal{E}_T$ denote the sets of faces and edges of polyhedron T, respectively. For every cell T in $\mathcal{T}$, we define the collocation point $\mathbf{x}_T$ at the barycenter of T. Finally, we denote by Σ_T the set of nearby collocation points of the cell T, and by $\Sigma_{f,T}$ the set of nearby collocation points of the face $f \in \mathcal{F}_T$ [5, 16].

We assume that for every cell–face pair $T \to f$, $T \in \mathcal{T}$, $f \in \mathcal{F}_T$, there exist three points $\mathbf{x}_{f,1}$, $\mathbf{x}_{f,2}$, and $\mathbf{x}_{f,3}$ in set Σ_T such that the following condition is held (see Fig. 2):

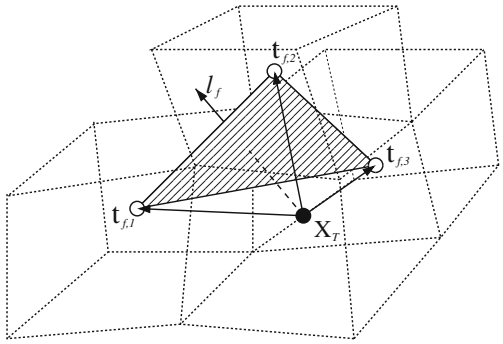

Fig. 2 Co-normal vector and vector triplet

The co-normal vector $\boldsymbol{\ell}_f = \mathbb{K}(\mathbf{x}_f)\mathbf{n}_f$ started from $\mathbf{x}_T$ belongs to the trihedral corner formed by vectors

$$\mathbf{t}_{f,1} = \mathbf{x}_{f,1} - \mathbf{x}_T, \quad \mathbf{t}_{f,2} = \mathbf{x}_{f,2} - \mathbf{x}_T, \quad \mathbf{t}_{f,3} = \mathbf{x}_{f,3} - \mathbf{x}_T, \tag{9}$$

and

$$\frac{1}{|\boldsymbol{\ell}_f|}\boldsymbol{\ell}_f = \frac{\alpha_f}{|\mathbf{t}_{f,1}|}\mathbf{t}_{f,1} + \frac{\beta_f}{|\mathbf{t}_{f,2}|}\mathbf{t}_{f,2} + \frac{\gamma_f}{|\mathbf{t}_{f,3}|}\mathbf{t}_{f,3}, \tag{10}$$

where $\alpha_f \geq 0, \beta_f \geq 0, \gamma_f \geq 0$.

The coefficients $\alpha_f, \beta_f, \gamma_f$ are computed as follows:

$$\alpha_f = \frac{A_{f,1}}{A_f}, \qquad \beta_f = \frac{A_{f,2}}{A_f}, \qquad \gamma_f = \frac{A_{f,3}}{A_f}, \tag{11}$$

where

$$A_f = \frac{|\mathbf{t}_{f,1}\mathbf{t}_{f,2}\mathbf{t}_{f,3}|}{|\mathbf{t}_{f,1}||\mathbf{t}_{f,2}||\mathbf{t}_{f,3}|}, \quad A_{f,1} = \frac{|\boldsymbol{\ell}_f\mathbf{t}_{f,2}\mathbf{t}_{f,3}|}{|\boldsymbol{\ell}_f||\mathbf{t}_{f,2}||\mathbf{t}_{f,3}|}$$

$$A_{f,2} = \frac{|\mathbf{t}_{f,1}\boldsymbol{\ell}_f\mathbf{t}_{f,3}|}{|\mathbf{t}_{f,1}||\boldsymbol{\ell}_f||\mathbf{t}_{f,3}|}, \quad A_{f,3} = \frac{|\mathbf{t}_{f,1}\mathbf{t}_{f,2}\boldsymbol{\ell}_f|}{|\mathbf{t}_{f,1}||\mathbf{t}_{f,2}||\boldsymbol{\ell}_f|}$$

and $|\mathbf{a}\ \mathbf{b}\ \mathbf{c}| = |(\mathbf{a} \times \mathbf{b}) \cdot \mathbf{c}|$.

Similarly, we assume that for every face–cell pair $f \to T$, $f \in \mathcal{F}_B \cup \mathcal{F}_J$, $T : f \in \mathcal{F}_T$, there exist three points $\mathbf{x}_{f,1}$, $\mathbf{x}_{f,2}$, and $\mathbf{x}_{f,3}$ in set $\Sigma_{f,T}$ such that the vector $\boldsymbol{\ell}_{f,T} = -\mathbb{K}_T(\mathbf{x}_f)\mathbf{n}_f$ started from $\mathbf{x}_f$ belongs to the trihedral corner formed by vectors

$$\mathbf{t}_{f,1} = \mathbf{x}_{f,1} - \mathbf{x}_f, \quad \mathbf{t}_{f,2} = \mathbf{x}_{f,2} - \mathbf{x}_f, \quad \mathbf{t}_{f,3} = \mathbf{x}_{f,3} - \mathbf{x}_f, \tag{12}$$

and Eqs. 10–11 hold true.

Let f be an interior face. The case of boundary face is considered in detail in [5, 16] and is not addressed here. We denote by T_+ and T_- the cells that share f and assume that $\mathbf{n}_f$ is outward for T_+. Let $\mathbf{x}_\pm$ (or $\mathbf{x}_{T_\pm}$) be the collocation points of $T_\pm$. Let $C_\pm$ (or $C_{T_\pm}$) be the discrete concentrations in $T_\pm$.

We begin with the case $f \notin \mathcal{F}_J$ and introduce $\mathbb{K}_f = \mathbb{K}(\mathbf{x}_f)$. Let $T = T_+$. Using the above notations, definition of the directional derivative,

$$\frac{\partial c}{\partial \boldsymbol{\ell}_f}|\boldsymbol{\ell}_f| = \nabla c \cdot (\mathbb{K}_f\,\mathbf{n}_f),$$

and assumption (10), we write

$$\begin{aligned}\mathbf{q}_f \cdot \mathbf{n}_f &= -\frac{|\boldsymbol{\ell}_f|}{|f|}\int_f \frac{\partial c}{\partial \boldsymbol{\ell}_f}\,\mathrm{d}s \\ &= -\frac{|\boldsymbol{\ell}_f|}{|f|}\int_f \left(\alpha_f\frac{\partial c}{\partial \mathbf{t}_{f,1}} + \beta_f\frac{\partial c}{\partial \mathbf{t}_{f,2}} + \gamma_f\frac{\partial c}{\partial \mathbf{t}_{f,3}}\right)\mathrm{d}s.\end{aligned} \tag{13}$$

Replacing directional derivatives with finite differences, we get

$$\int_f \frac{\partial c}{\partial \mathbf{t}_{f,i}}\,\mathrm{d}s = \frac{C_{f,i} - C_T}{|\mathbf{x}_{f,i} - \mathbf{x}_T|}\,|f| + O(h_T^3), \quad i = 1, 2, 3, \tag{14}$$

where h_T is the diameter of cell T. Using the finite difference approximations (14), we transform formula (13) to

$$\begin{aligned}\mathbf{q}_f^h \cdot \mathbf{n}_f = -|\boldsymbol{\ell}_f|\Bigg(&\frac{\alpha_f}{|\mathbf{t}_{f,1}|}(C_{f,1} - C_T) \\ &+ \frac{\beta_f}{|\mathbf{t}_{f,2}|}(C_{f,2} - C_T) + \frac{\gamma_f}{|\mathbf{t}_{f,3}|}(C_{f,3} - C_T)\Bigg).\end{aligned} \tag{15}$$

At the moment, this flux involves four rather than two concentrations. To derive a two-point flux approximation, we consider the cell T_- and derive another approximation of flux through face f. To distinguish between T_+ and T_-, we add subscripts $\pm$ and omit subscript f. Since $\mathbf{n}_f$ is the inward normal vector for T_-, we have to change sign of the right-hand side:

$$\begin{aligned}\mathbf{q}_\pm^h \cdot \mathbf{n}_f = \mp\,|\boldsymbol{\ell}_f|\Bigg(&\frac{\alpha_\pm}{|\mathbf{t}_{\pm,1}|}\,(C_{\pm,1} - C_\pm) \\ &+ \frac{\beta_\pm}{|\mathbf{t}_{\pm,2}|}\,(C_{\pm,2} - C_\pm) + \frac{\gamma_\pm}{|\mathbf{t}_{\pm,3}|}\,(C_{\pm,3} - C_\pm)\Bigg),\end{aligned} \tag{16}$$

where $\alpha_\pm$, $\beta_\pm$, and $\gamma_\pm$ are given by Eq. 11 and $C_{\pm,i}$ denote concentrations at points $\mathbf{x}_{\pm,i}$ from $\Sigma_{T_\pm}$.

We define a new discrete diffusive flux as a linear combination of $\mathbf{q}_\pm^h \cdot \mathbf{n}_f$ with nonnegative weights $\mu_\pm$:

$$\begin{aligned}\mathbf{q}_f^h \cdot \mathbf{n}_f =& \mu_+\,\mathbf{q}_+^h \cdot \mathbf{n}_f + \mu_-\,\mathbf{q}_-^h \cdot \mathbf{n}_f \\ =& \mu_+|\boldsymbol{\ell}_f|\left(\frac{\alpha_+}{|\mathbf{t}_{+,1}|} + \frac{\beta_+}{|\mathbf{t}_{+,2}|} + \frac{\gamma_+}{|\mathbf{t}_{+,3}|}\right)C_+ \\ &- \mu_-|\boldsymbol{\ell}_f|\left(\frac{\alpha_-}{|\mathbf{t}_{-,1}|} + \frac{\beta_-}{|\mathbf{t}_{-,2}|} + \frac{\gamma_-}{|\mathbf{t}_{-,3}|}\right)C_- \\ &- \mu_+|\boldsymbol{\ell}_f|\left(\frac{\alpha_+}{|\mathbf{t}_{+,1}|}C_{+,1} + \frac{\beta_+}{|\mathbf{t}_{+,2}|}C_{+,2} + \frac{\gamma_+}{|\mathbf{t}_{+,3}|}C_{+,3}\right) \\ &+ \mu_-|\boldsymbol{\ell}_f|\left(\frac{\alpha_-}{|\mathbf{t}_{-,1}|}C_{-,1} + \frac{\beta_-}{|\mathbf{t}_{-,2}|}C_{-,2} + \frac{\gamma_-}{|\mathbf{t}_{-,3}|}C_{-,3}\right).\end{aligned} \tag{17}$$

The obvious requirement for the weights is to cancel the terms in the last two rows of Eq. 17 which results in a two-point flux formula. The second requirement is to

approximate the true flux. These requirements lead us to the following system

$$\begin{cases} -\mu_+ d_+ + \mu_- d_- = 0, \\ \mu_+ + \mu_- = 1, \end{cases} \tag{18}$$

where

$$d_\pm = |\boldsymbol{\ell}_f| \left(\frac{\alpha_\pm}{|\mathbf{t}_{\pm,1}|} C_{\pm,1} + \frac{\beta_\pm}{|\mathbf{t}_{\pm,2}|} C_{\pm,2} + \frac{\gamma_\pm}{|\mathbf{t}_{\pm,3}|} C_{\pm,3} \right).$$

Since coefficients $d_\pm$ depend on both geometry and concentration, the weights $\mu_\pm$ do as well. Thus, the resulting TPFA is *nonlinear*.

Remark 1 It may happen that concentration $C_{+,i}$, $(C_{-,i})$ $i = 1, 2, 3$, is defined at the same collocation point as C_- (C_+). In this case, the terms to be cancelled are changed so that they do not incorporate $C_\pm$. By doing so, for the Laplace operator, we recover the classical linear scheme with the 6-1-1-1-1-1-1 stencil on uniform cubic meshes.

The solution of Eq. 18 can be written explicitly. In all cases $d_\pm \geq 0$ if $C \geq 0$. If $d_\pm = 0$, we set $\mu_+ = \mu_- = \frac{1}{2}$. Otherwise,

$$\mu_+ = \frac{d_-}{d_- + d_+} \qquad \text{and} \qquad \mu_- = \frac{d_+}{d_- + d_+}.$$

This implies that the weights $\mu_\pm$ are nonnegative. Substituting this into Eq. 17, we get the two-point flux formula (5) with nonnegative coefficients

$$D^\pm = \mu_\pm |\boldsymbol{\ell}_f| (\alpha_\pm / |\mathbf{t}_{\pm,1}| + \beta_\pm / |\mathbf{t}_{\pm,2}| + \gamma_\pm / |\mathbf{t}_{\pm,3}|). \tag{19}$$

Now, we consider the case $f \in \mathcal{F}_J$ when $\mathbb{K}_+(\mathbf{x}_f)$ and $\mathbb{K}_-(\mathbf{x}_f)$ differ, where

$$\mathbb{K}_\pm(\mathbf{x}_f) = \lim_{\mathbf{x} \in \mathcal{T}_\pm,\ \mathbf{x} \to \mathbf{x}_f} \mathbb{K}(\mathbf{x}).$$

We derive the nonlinear TPFAs in cells T_+ and T_- independently using auxiliary unknown C_f collocated at $\mathbf{x}_f$:

$$\left(\mathbf{q}_f^h \cdot \mathbf{n}_f \right)_+ = N^+ C_+ - N_f^+ C_f, \tag{20}$$

$$-\left(\mathbf{q}_f^h \cdot \mathbf{n}_f \right)_- = N^- C_- - N_f^- C_f. \tag{21}$$

Nonnegative coefficients N^+, N_f^+, N^-, N_f^- are derived similarly to coefficients (19) on the basis of discrete concentrations at collocation points from $\Sigma_{T_\pm}$, $\Sigma_{f,T_\pm}$ and $\boldsymbol{\ell}_\pm = \mp \mathbb{K}_\pm(\mathbf{x}_f)\, \mathbf{n}_f$, the co-normal vectors to face f outward with respect to $T_\pm$. Continuity of the normal component of the diffusive flux allows us to eliminate C_f from Eqs. 20–21

$$C_f = \left(N^+ C_+ + N^- C_- \right) / \left(N_f^+ + N_f^- \right) \tag{22}$$

and derive nonlinear TPFA (5) with coefficients

$$D^\pm = N^\pm N_f^\mp / \left(N_f^+ + N_f^- \right). \tag{23}$$

If both $N_f^\pm = 0$, we set $D^\pm = N^\pm/2$ and $C_f = (C_+ + C_-)/2$.

In Section 3.2, we shall need the variation of coefficients $D^\pm$ in Eq. 19 to calculate Jacobian matrix. First, we write variations for $d_\pm$ and $\mu_\pm$:

$$\Delta d_\pm = |\boldsymbol{\ell}_f| \left(\frac{\alpha_\pm}{|\mathbf{t}_{\pm,1}|} \Delta C_{\pm,1} + \frac{\beta_\pm}{|\mathbf{t}_{\pm,2}|} \Delta C_{\pm,2} + \frac{\gamma_\pm}{|\mathbf{t}_{\pm,3}|} \Delta C_{\pm,3} \right), \tag{24}$$

$$\Delta \mu_\pm = \frac{\Delta d_\mp}{d_\mp + d_\pm} - (\Delta d_\mp + \Delta d_\pm) \frac{d_\mp}{(d_\mp + d_\pm)^2}. \tag{25}$$

Then for the variation of $D^\pm$, we have the linear combination:

$$\begin{aligned} \Delta D^\pm &= \Delta \mu_\pm \left(\alpha_\pm / |\mathbf{t}_{\pm,1}| + \beta_\pm / |\mathbf{t}_{\pm,2}| + \gamma_\pm / |\mathbf{t}_{\pm,3}| \right) \\ &= \sum_{T_i \in \Sigma_{T_*}} L_i^\pm \Delta C_i, \end{aligned} \tag{26}$$

where $\Sigma_{T_*} := \Sigma_{T_+} \cup \Sigma_{T_-}$ and $L_i^\pm = L_i^\pm(C)$ are the coefficients of the linear combination obtained by substituting Eqs. 24 and 25 into Eq. 19.

2.3 Nonlinear discrete system

For every T in $\mathcal{T}$, the cell Eq. 4 is

$$\sum_{f \in \mathcal{F}_T} \chi(T, f)\, \mathbf{q}_f^h \cdot \mathbf{n}_f = \int_T f \, \mathrm{d}x, \tag{27}$$

where $\chi(T, f) = sign(\mathbf{n}_f \cdot \mathbf{n}_T(\mathbf{x}_f))$. Substituting two-point flux formula (5) with nonnegative coefficients given by Eqs. 19 and 23 into Eq. 27, we get a nonlinear system of $N_\mathcal{T}$ equations

$$\mathbf{M}\, C = G. \tag{28}$$

The matrix $\mathbf{M} = \mathbf{M}(C)$ with elements depending on C may be represented by assembling of 2×2 matrices

$$\mathbf{M}_f = \begin{pmatrix} D^+ & -D^- \\ -D^+ & D^- \end{pmatrix} \tag{29}$$

for the interior faces and 1×1 matrices $\mathbf{M}_f(C) = D^+$ for Dirichlet faces. The right-hand side vector $G = G(C)$ is generated by the source and the boundary data. The system (28) is solved by, e.g., Picard method that contains two nested iterations, the nonlinear outer iterations and inner iterations for linearized systems.

3 Two-phase flow model

For the sake of simplicity, we consider the two-phase flow in a porous medium [2, 4]; as for the three-phase flow, the

effect of using linear or nonlinear discretization scheme is the same. The phase that wets the medium more than the other is called wetting phase and is indicated by subscript w. The other phase is the nonwetting phase and indicated by o.

The basic equations for the two-phase flow are the following:

1. Mass conservation for each phase:

$$\frac{\partial}{\partial t}\frac{\phi S_\alpha}{B_\alpha} = -\mathrm{div}\mathbf{u}_\alpha + q_\alpha, \quad \alpha = w, o. \tag{30}$$

2. Darcy's law:

$$\mathbf{u}_\alpha = -\lambda_\alpha \mathbb{K}(\nabla p_\alpha - \rho_\alpha g \nabla z), \quad \alpha = w, o. \tag{31}$$

3. Two fluids fill the voids:

$$S_w + S_o = 1. \tag{32}$$

4. Pressure difference between phases is given by capillary pressure $p_c = p_c(S_w)$:

$$p_o - p_w = p_c, \tag{33}$$

where $\mathbb{K}$ is an absolute permeability tensor, ϕ is the porosity, g is the gravity term, z is the depth; in the phase α: p_α is unknown pressure, S_α is unknown saturation, $\mathbf{u}_\alpha$ is unknown Darcy's velocity, ρ_α is unknown density, $B_\alpha = \rho_{\alpha,0}/\rho_\alpha$ is the formation volume factor, μ_α is the viscosity, $k_{r\alpha}$ is the relative phase permeability, $\lambda_\alpha = k_{r\alpha}/(\mu_\alpha B_\alpha)$ is the mobility, q_α is the source/sink well term.

We choose oil pressure p_o and water saturation S_w as primary unknowns $(p, S) \equiv (p_o, S_w)$. In the sequel, we also take into account the following dependencies: $k_{r\alpha} = k_{r\alpha}(S_w)$, $\mu_\alpha = \mu_\alpha(p_o)$, $B_\alpha = B_\alpha(p_o)$, and $\phi = \phi_0\left(1 + c_R\left(p_o - p_o^0\right)\right)$.

We have no-flow (homogeneous Neumann) boundary condition on the reservoir boundary. Wells are incorporated through the well terms in Eq. 30. Each well is assumed to be vertical and connected to the center of a cell. The formula for the well term was suggested by Peaceman [19]. For a cell T with center $\mathbf{x}_T$ connected to the well, we have:

$$q_\alpha = \frac{\rho_\alpha k_{r\alpha}}{\mu_\alpha} WI\Big(p_{\mathrm{bh}} - p - \rho_\alpha(z_{\mathrm{bh}} - z)\Big)\delta(\mathbf{x} - \mathbf{x}_T), \tag{34}$$

where p_{bh} is a given bottom hole pressure, WI is a well index which does not depend on the properties of fluids but depends on properties of the media, $\delta(\mathbf{x} - \mathbf{x}_T)$ is the Dirac function.

3.1 IMPES time stepping

In this section, we recall the IMPES time stepping for two-phase flow model. Let the total velocity be $\mathbf{u} = \mathbf{u}_o + \mathbf{u}_w$.

If the rock porosity and liquid densities are fixed during the time step, we have $\frac{\partial S_o}{\partial t} + \frac{\partial S_w}{\partial t} = 0$ and then

$$\mathrm{div}\mathbf{u} = q_w + q_o. \tag{35}$$

Applying Eq. 33 to Eq. 31 gives

$$\mathbf{u} = -\mathbb{K}\big(\lambda\nabla p - \lambda_w \nabla p_c - (\lambda_w\rho_w + \lambda_o\rho_o)g\nabla z\big), \tag{36}$$

where $\lambda = \lambda_w + \lambda_o$ is the total mobility.

Substituting Eq. 36 into Eq. 35 gives the pressure equation

$$\begin{aligned} &-\mathrm{div}(\mathbb{K}\lambda\nabla p) = q_w + q_o \\ &-\mathrm{div}\big[\mathbb{K}\big(\lambda_w\nabla p_c + (\lambda_w\rho_w + \lambda_o\rho_o)g\nabla z\big)\big]. \end{aligned} \tag{37}$$

The phase velocities $\mathbf{u}_w$ and $\mathbf{u}_o$ can be expressed through the total velocity $\mathbf{u}$ by

$$\mathbf{u}_w = \frac{\lambda_w}{\lambda}\big(\mathbf{u} + \mathbb{K}\lambda_o\nabla p_c + \mathbb{K}\lambda_o(\rho_w - \rho_o)g\nabla z\big),$$

$$\mathbf{u}_o = \frac{\lambda_o}{\lambda}\big(\mathbf{u} - \mathbb{K}\lambda_w\nabla p_c + \mathbb{K}\lambda_w(\rho_o - \rho_w)g\nabla z\big).$$

Similarly, Eqs. 33 and 36 applied to Eqs. 30 and 31 (for $\alpha = w$) yield the saturation equation

$$\begin{aligned} &\mathrm{div}\frac{\lambda_w}{\lambda}\left[\mathbf{u} + \mathbb{K}\lambda_o\left(\frac{dp_c}{dS}\nabla S + (\rho_o - \rho_w)g\nabla z\right)\right] \\ &+ \phi\frac{\partial S}{\partial t} = q_w. \end{aligned} \tag{38}$$

Finally, the IMPES method can be formalized:

1. Solve **implicitly** (37) to obtain current pressure p^n from current saturation S^n:

$$\begin{aligned} &-\mathrm{div}(\mathbb{K}\lambda^n\nabla p^n) = q_w + q_o \\ &= -\mathrm{div}\big[\mathbb{K}\big(\lambda_w^n\nabla p_c + (\lambda_w^n\rho_w^n + \lambda_o^n\rho_o^n)g\nabla z\big)\big], \end{aligned} \tag{39}$$

where $\lambda_\alpha^n = \lambda_\alpha(S^n, p^n)$ and $\rho_\alpha^n = \rho_\alpha(p^n)$.

2. Use Eq. 36 to find current Darcy's velocity $\mathbf{u}^n$ using current S^n and p^n:

$$\mathbf{u}^n = -\mathbb{K}\big(\lambda^n\nabla p^n - \lambda_w^n\nabla p_c - (\lambda_w^n\rho_w^n + \lambda_o^n\rho_o^n)g\nabla z\big). \tag{40}$$

3. Solve **explicitly** (38) to get the next time step saturation S^{n+1} using current S^n, p^n, and u^n:

$$\begin{aligned} &\frac{1}{\Delta t^{n+1}}\left[\left(\frac{\phi S}{B_w}\right)^{n+1} - \left(\frac{\phi S}{B_w}\right)^n\right] = q_w \\ &-\mathrm{div}\frac{\lambda_w^n}{\lambda^n}\left[\mathbb{K}\lambda_o^n\left(\frac{dp_c}{dS}\nabla S + (\rho_o^n - \rho_w^n)g\nabla z\right) + \mathbf{u}^n\right]. \end{aligned} \tag{41}$$

Note that the Eq. 39 is a stationary diffusion equation with diffusion tensor $\mathbb{K}\lambda^n$. Discretization of diffusion fluxes in Eq. 39, as well as computation of the right-hand sides

of Eqs. 40 and 41 is based on the nonlinear TPFA substituting concentration for pressures p_o, p_c, or z. The use of Picard method for the solution of Eq. 39 with lagging coefficients from previous nonlinear iteration allows us to take all coefficients in Eq. 39 implicitly: λ^n, λ_w^n, λ_o^n, ρ_w^n, ρ_o^n.

In the discrete counterpart of Eqs. 39–41 the mobility $\lambda_\alpha = \frac{k_{r\alpha}(S)}{B_\alpha(p)\mu_\alpha(p)}$ on face f_{ij} is taken upwinded:

$$\lambda_\alpha = \begin{cases} \lambda_\alpha(S_i, p_i) & \text{if flow is directed from cell } i \text{ to } j, \\ \lambda_\alpha(S_j, p_j) & \text{if flow is directed from cell } j \text{ to } i. \end{cases}$$

If a cell contains a well, the phase mobilities are taken from the well cells. In case of the injector well, we have only water injected and thus take the downstream mobility:

$$\lambda_{\text{injector}} = \left(\frac{k_{rw}}{B_w\mu_w} + \frac{k_{ro}}{B_o\mu_o}\right)_{\text{cell}}.$$

It is assumed that there is no capillary pressure in wells, so both water and oil fluxes depend on the same (oil) pressure.

3.2 Fully implicit scheme

Another time discretization technique widely used in reservoir simulation is the fully implicit scheme. First, we apply the implicit scheme to the mass conservation Eq. 30:

$$\frac{\left(\frac{\phi S_\alpha}{B_\alpha}\right)^{n+1} - \left(\frac{\phi S_\alpha}{B_\alpha}\right)^{n}}{\Delta t^{n+1}} = -\operatorname{div}\mathbf{u}_\alpha^{n+1} + q_\alpha^{n+1}, \quad \alpha = w, o. \tag{42}$$

Now, we can define the nonlinear residual for the l^{th} approximation to a quantity evaluated at time step $n+1$ inside grid cell T_i:

$$R_{\alpha,i} = \int_{T_i}\left[\left(\frac{\phi S_\alpha}{B_\alpha}\right)_i^l - \left(\frac{\phi S_\alpha}{B_\alpha}\right)_i^n + \Delta t^{n+1}\left(\operatorname{div}\mathbf{u}_\alpha^l - q_\alpha^l\right)\right]\mathrm{d}x, \quad \alpha = w, o. \tag{43}$$

The discrete counterpart of Eq. 42 can be written as:

$$R_{\alpha,i} = 0, \quad \alpha = w, o \tag{44}$$

for all grid cells T_i at every time step.

The combination of Eqs. 31, 43, and 44 generates a nonlinear system which is usually solved by Newton method:

$$J\left(x^l\right)\delta x^l = -R\left(x^l\right), \tag{45}$$

$$x^{l+1} = x^l + \delta x^l, \tag{46}$$

where l is the l^{th} Newton step, $x = (p_o S_w)^T$ is a vector of primary unknowns in all grid cells, $R(x) = (R_w(x) R_o(x))^T$ is a vector of nonlinear residuals in all grid cells, and J is the Jacobian matrix:

$$J(x) = \begin{pmatrix} \frac{\partial R_w}{\partial p_o}(x) & \frac{\partial R_w}{\partial S_w}(x) \\ \frac{\partial R_o}{\partial p_o}(x) & \frac{\partial R_o}{\partial S_w}(x) \end{pmatrix}.$$

We terminate Newton's method when the norm of the residual vector drops below ε_{nwt}.

The construction of Jacobian matrix is as follows. We divide the residual into two parts: accumulation (including well terms) and transport, $R_{\alpha,i} = R_{\alpha,i}^{\text{acc}} + R_{\alpha,i}^{\text{trans}}$, where:

$$R_{\alpha,i}^{\text{acc}} = V_i\left[\left(\frac{\phi S_\alpha}{B_\alpha}\right)^{l,i} - \left(\frac{\phi S_\alpha}{B_\alpha}\right)^{n,i}\right] - \Delta t^{n+1} Q_\alpha^{l,i},$$

$$Q_\alpha^{l,i} = \int_{T_i} q_\alpha^l dx,$$

$$R_{\alpha,i}^{\text{trans}} = \Delta t^{n+1}\int_{T_i}\operatorname{div}\mathbf{u}_\alpha^l\,\mathrm{d}x, \quad \alpha = w, o.$$

3.2.1 Accumulation term

First, we consider the variation of the accumulation term:

$$\Delta R_{w,i}^{\text{acc}} = V_i\,\Delta\left(\frac{\phi S_w}{B_w}\right) - \Delta t^{n+1}\Delta Q_w,$$

$$\Delta R_{o,i}^{\text{acc}} = V_i\,\Delta\left(\frac{\phi S_o}{B_o}\right) - \Delta t^{n+1}\Delta Q_o,$$

where

$$\Delta\left(\frac{\phi S_w}{B_w}\right) = \frac{\phi}{B_w}\Delta S_w + S_w\left(\frac{\phi_0 c_R}{B_w} - \frac{\phi}{B_w^2}\frac{dB_w}{dp_o}\right)\Delta p_o,$$

$$\Delta\left(\frac{\phi S_o}{B_o}\right) = -\frac{\phi}{B_o}\Delta S_w + (1-S_w)\left(\frac{\phi_0 c_R}{B_o} - \frac{\phi}{B_o^2}\frac{dB_o}{dp_o}\right)\Delta p_o.$$

For the wells, we first define auxiliary variables and derivatives:

$$\mathcal{D}_\alpha = p_{\text{bh}} - p_o - \frac{\rho_{\alpha,0}}{B_\alpha}g(z_{\text{bh}} - z),$$

$$\frac{d\mathcal{D}_\alpha}{dp_o} = -1 + \frac{\rho_{\alpha,0}}{B_\alpha^2}\frac{dB_\alpha}{dp_o}g(z_{\text{bh}} - z), \qquad \frac{d\lambda_\alpha}{dS_w} = \frac{dk_{r\alpha}}{dS_w}\frac{1}{B_\alpha\mu_\alpha},$$

$$\frac{d\lambda_\alpha}{dp_o} = -k_{r\alpha}\left(B_\alpha\frac{d\mu_\alpha}{dp_o} + \mu_\alpha\frac{dB_\alpha}{dp_o}\right)/(B_\alpha\mu_\alpha)^2, \quad \alpha = w, o.$$

Then the variation of the well term is: for the producer well

$$\Delta Q_\alpha = WI\left[\mathcal{D}_\alpha\frac{d\lambda_\alpha}{dS_w}\Delta S_w + \left(\lambda_\alpha\frac{d\mathcal{D}_\alpha}{dp_o} + \frac{d\lambda_\alpha}{dp_o}\mathcal{D}_\alpha\right)\Delta p_o\right]$$

and for the injector well

$$\Delta Q_w = WI\left[\mathcal{D}_w\left(\frac{d\lambda_w}{dS_w}+\frac{d\lambda_o}{dS_w}\right)\Delta S_w + \left((\lambda_w+\lambda_o)\frac{d\mathcal{D}_w}{dp_o}+\mathcal{D}_w\left(\frac{d\lambda_w}{dp_o}+\frac{d\lambda_o}{dp_o}\right)\right)\Delta p_o\right],$$
$$\Delta Q_o = 0.$$

3.2.2 Transport term

Now, we consider the transport term composed of Darcy fluxes

$$R^{\text{trans}}_{\alpha,i} = \Delta t^{n+1}\int_{\partial T_i}(\mathbf{u}_\alpha\cdot\mathbf{n})\,\mathrm{d}s \approx \Delta t^{n+1}\sum_{f\in\partial T_i}\mathbf{u}^h_{\alpha,f}\cdot\mathbf{n}_f. \tag{47}$$

We apply TPFA for the flux of each field: p_o, p_c, z and denote the respective flux coefficients by $D^{\pm}_p$, $D^{\pm}_{p_c}$, $D^{\pm}_z$ and the collocated field values at $\mathbf{x}_{T_\pm}$ by $p^{\pm}_o$, $p^{\pm}_c$, $S^{\pm}_w$, $z^{\pm}$. In this case,

$$\begin{aligned}\mathbf{u}^h_{w,f}\cdot\mathbf{n}_f =& -\left(\frac{k_{rw}}{\mu_w B_w}\right)_f\left(D^+_p p^+_o - D^-_p p^-_o\right)\\ &+\left(\frac{k_{rw}}{\mu_w B_w}\right)_f\left(D^+_{p_c} p^+_c - D^-_{p_c} p^-_c\right)\\ &+\left(\frac{k_{rw}}{\mu_w B^2_w}\right)_f\left[\rho_{w,0}\,g\left(D^+_z z^+ - D^-_z z^-\right)\right],\end{aligned} \tag{48}$$

$$\begin{aligned}\mathbf{u}^h_{o,f}\cdot\mathbf{n}_f =& -\left(\frac{k_{ro}}{\mu_o B_o}\right)_f\left(D^+_p p^+_o - D^-_p p^-_o\right)\\ &+\left(\frac{k_{ro}}{\mu_o B^2_o}\right)_f\left[\rho_{o,0}\,g\left(D^+_z z^+ - D^-_z z^-\right)\right].\end{aligned} \tag{49}$$

Here, $k_{r\alpha} = k_{r\alpha}(\widetilde{S}_w)$, $\widetilde{S}_w$ is the upwinded value of water saturation on face f and $B_\alpha = B_\alpha(\widetilde{p}_o)$, $\mu_\alpha = \mu_\alpha(\widetilde{p}_o)$, $\widetilde{p}_o$ is the upwinded value of oil pressure on face f.

Table 1 Fluid compressibility properties

p (psia)	B_o $\left(\frac{\text{bbl}}{\text{STB}}\right)$	B_w $\left(\frac{\text{bbl}}{\text{STB}}\right)$	μ_o (cp)	μ_w (cp)
3,900	1.0030	1.01317	90.6	0.515
4,000	1.0020	1.01291	96.0	0.518
4,100	1.0009	1.01264	101.7	0.521

We define auxiliary variables and derivatives:

$$\lambda_{g,\alpha} = \frac{k_{r\alpha}}{\mu_w B^2_w}, \qquad \frac{d\lambda_{g,\alpha}}{d\widetilde{S}_w} = \frac{d\lambda_\alpha}{d\widetilde{S}_w}/B_w,$$

$$\frac{d\lambda_{g,\alpha}}{d\widetilde{p}_o} = \left(\frac{d\lambda_\alpha}{d\widetilde{p}_o}B_w - \lambda_\alpha\frac{dB_w}{d\widetilde{p}_o}\right)/B^2_w, \quad \alpha = w, o,$$

$$\mathcal{D}_1 = D^+_p p^+_o - D^-_p p^-_o,$$

$$\mathcal{D}_2 = D^+_{p_c} p^+_c - D^-_{p_c} p^-_c,$$

$$\mathcal{D}_{3,\alpha} = \rho_{\alpha,0}\,g\left(D^+_z z^+ - D^-_z z^-\right).$$

Using Eqs. 48 and 49, we get the following representation for the flux variation for each of two phases:

$$\begin{aligned}\Delta\left(\mathbf{u}^h_{w,f}\cdot\mathbf{n}_f\right) =& \left[\left(\frac{d\lambda_w}{d\widetilde{S}_w}\right)(-\mathcal{D}_1+\mathcal{D}_2)+\frac{d\lambda_{g,w}}{d\widetilde{S}_w}\mathcal{D}_{3,w}\right]\Delta\widetilde{S}_w\\ &+\left[\left(\frac{d\lambda_w}{d\widetilde{p}_o}\right)(-\mathcal{D}_1+\mathcal{D}_2)+\frac{d\lambda_{g,w}}{d\widetilde{p}_o}\mathcal{D}_{3,w}\right]\Delta\widetilde{p}_o\\ &-\lambda_w\left(D^+_p\Delta p^+_o - D^-_p\Delta p^-_o\right)\\ &+\lambda_w\left(D^+_{p_c}\left(\frac{dp_c}{dS_w}\right)^+\Delta S^+_w - D^-_{p_c}\left(\frac{dP_c}{dS_w}\right)^-\Delta S^-_w\right)\\ &-\lambda_w\left(\Delta D^+_p p^+_o - \Delta D^-_p p^-_o\right)\\ &+\lambda_w\left(\Delta D^+_{p_c} p^+_c - \Delta D^-_{p_c} p^-_c\right),\end{aligned} \tag{50}$$

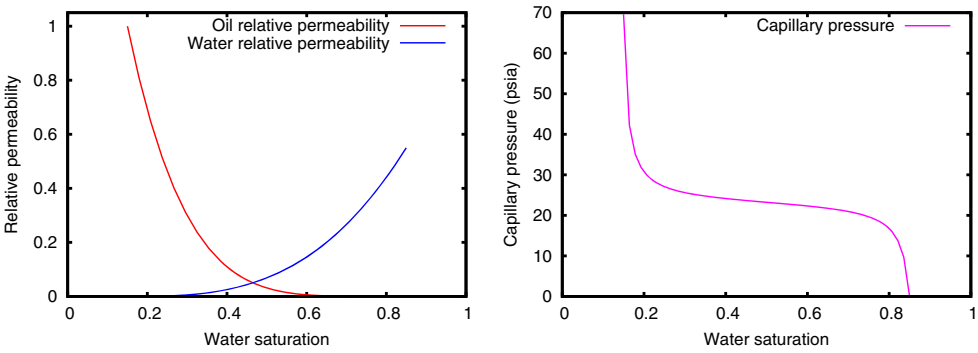

Fig. 3 *Left*: Oil and water relative permeabilities. *Right*: Capillary pressure dependence on S_w

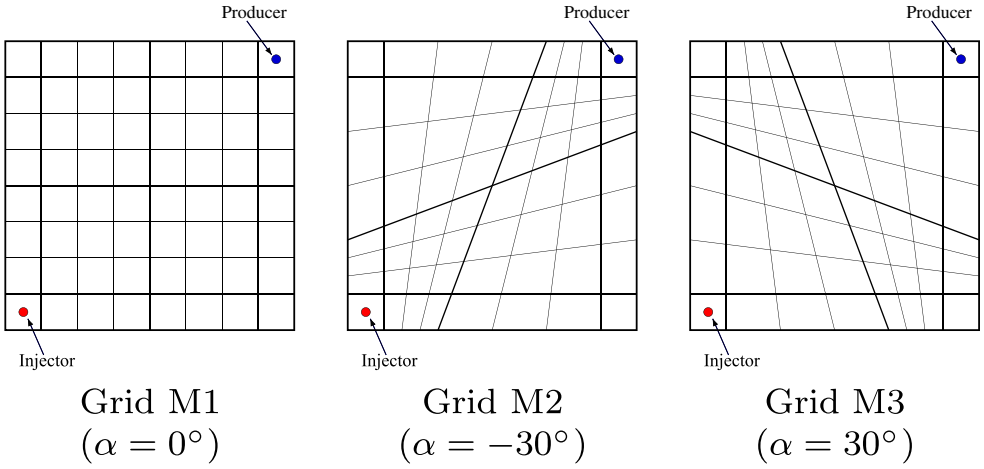

Fig. 4 Orthogonal and nonorthogonal sample grids

$$\Delta\left(\mathbf{u}^h_{o,f}\cdot\mathbf{n}_f\right)=\left[\left(\frac{d\lambda_o}{d\widetilde{S}_w}\right)(-\mathcal{D}_1+\mathcal{D}_2)+\frac{d\lambda_{g,o}}{d\widetilde{S}_w}\mathcal{D}_{3,o}\right]\Delta\widetilde{S}_w$$
$$+\left[\left(\frac{d\lambda_o}{d\widetilde{p}_o}\right)(-\mathcal{D}_1+\mathcal{D}_2)+\frac{d\lambda_{g,o}}{d\widetilde{p}_o}\mathcal{D}_{3,o}\right]\Delta\widetilde{p}_o$$
$$-\lambda_o\left(D_p^+\Delta p_o^+-D_p^-\Delta p_o^-\right)$$
$$+\lambda_o\left(\Delta D_p^+ p_o^+-\Delta D_p^- p_o^-\right). \tag{51}$$

Two possible approaches may be used to calculate the variation of the transport terms (50) and (51): coefficients $D_*^\pm$ may be assumed to be frozen for each Newton step [18, 22] or they may be differentiated as dependent of pressure and saturation in a few neighboring cells. In the first case, $\Delta D_*^\pm = 0$ and difference between the linear and nonlinear TPFAs is only in the way we calculate $D_*^\pm$, but not in sparsity of Jacobian matrix. The cost of each Jacobian-vector multiplication will remain the same for both linear and nonlinear TPFAs. If no coefficients are frozen in differentiation, then

$$\Delta D_p^\pm = \sum_{T_i\in\Sigma_{T_*}} L_{p,i}^\pm\,\Delta p_o^i, \tag{52}$$

$$\Delta D_{p_c}^\pm = \sum_{T_i\in\Sigma_{T_*}} L_{p_c,i}^\pm\left(\frac{dp_c}{dS_w}\right)^i\Delta S_w^i, \tag{53}$$

where $L_{p,i}^\pm$ and $L_{p_c,i}^\pm$ are the coefficients calculated in Eq. 26 for fields p_o and $p_c(S_w)$, respectively. This results in more dense Jacobian matrix and more expensive Jacobian-vector multiplication and preconditioning in the linear solve. To increase efficiency, one may consider a threshold which filters off small entries of the Jacobian matrix [22]. We shall not consider this option here.

4 Numerical experiments

In this section, we present a few numerical results obtained with the nonlinear TPFA for the two-phase flow model. The

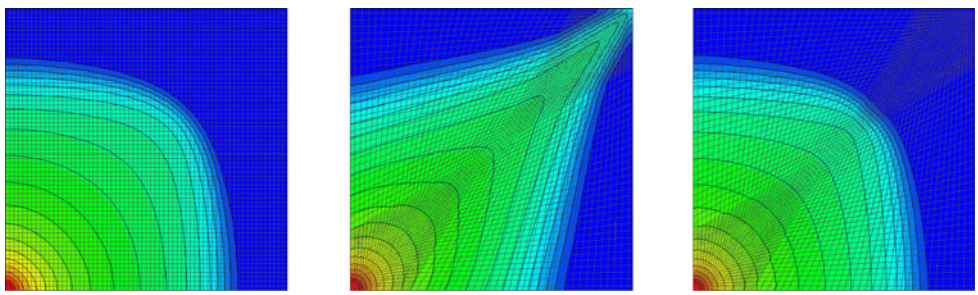

Fig. 5 Water saturation for grids M1 and M2 for the linear and nonlinear scheme at $T = 250$ days

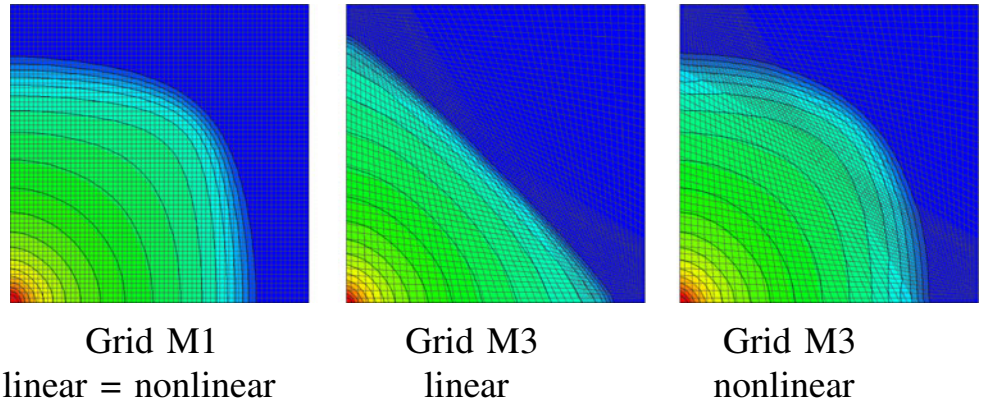

Fig. 6 Water saturation for grids M1 and M3 for the linear and nonlinear scheme at $T = 250$ days

accuracy and the computational cost of the method are compared with the ones for the conventional linear TPFA or MPFA. For the sake of brevity, we address here the fully implicit scheme only.

In the first two test cases, we consider pseudo-3D problems on $N \times N \times 1$ hexahedral meshes and use the following rock and fluid properties. Relative permeabilities of fluids $k_{r\alpha}$ are shown in Fig. 3 (left). Capillary pressure p_c dependence on S_w is presented in Fig. 3, right. Viscosities μ_α and volume factors B_α are set by Table 1, and densities are $\rho_{w,0} \approx 4.331 \times 10^{-1}$psi/ft and $\rho_{o,0} \approx 3.898 \times 10^{-1}$psi/ft. The rock is assumed to be incompressible.

Both wells are incorporated through the bottom hole pressures. For injector, it is $p_{\text{bh,inj}} = 4{,}100$ psia and for producer $p_{\text{bh,pr}} = 3{,}900$ psia. Well indexes are assumed to be fixed $WI = 10\,\frac{\text{bbl·cp}}{\text{day·psi}}$.

4.1 Nonorthogonal grid

The main idea of the first experiment as follows. Take uniform $32 \times 32 \times 1$ mesh. Fix the first and last two grid lines in order to leave well-connected cells intact. Rotate the central lines towards the wells (angle $\alpha = -30°$) or away from them ($\alpha = 30°$) and interpolate the other lines linearly between central lines and the boundary (see Fig. 4). Run simulation with the linear and nonlinear TPFAs on modified mesh and compare the results with the ones on the orthogonal mesh. Permeability tensor is chosen to be $\mathbb{K} = \{100, 100, 10\}$.

Table 2 Water breakthrough times (nonorthogonal grid)

	Grid M1	Grid M2	Grid M3
linear TPFA	372.2	224.1	564.2
nonlin.TPFA	372.2	362.2	388.5

Figure 5 shows water saturation field on orthogonal grid M1 (Fig. 5, left) and on grid M2 for the linear (Fig. 5, center) and nonlinear (Fig. 5, right) TPFAs. In case of linear discretization, the water front accelerates and its form differs from the one obtained on the orthogonal grid, while in case of nonlinear discretization, the fronts are almost equal.

Figure 6 shows water saturation field on orthogonal grid M1 (Fig. 6, left) and on grid M3 for the linear (Fig. 6, center) and nonlinear (Fig. 6, right) TPFAs. Again, nonlinear discretization provides the front which is very close to the front on the orthogonal grid, while the linear TPFA decelerates the water front.

The water breakthrough times are also noticeably different (see Table 2). Oil production rates are shown in Fig. 7. For grid M2 both linear and nonlinear fluxes break earlier than for grid M1, while for grid M3 both linear and nonlinear fluxes alternatively break later than for grid M1. Meanwhile, the breakthrough times for the nonlinear discretization on the modified grids are very close to the ones on the orthogonal grid.

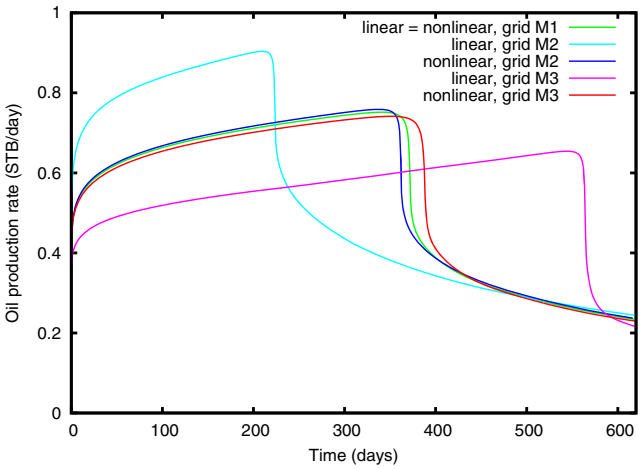

Fig. 7 Oil production rates for grids M1, M2, and M3

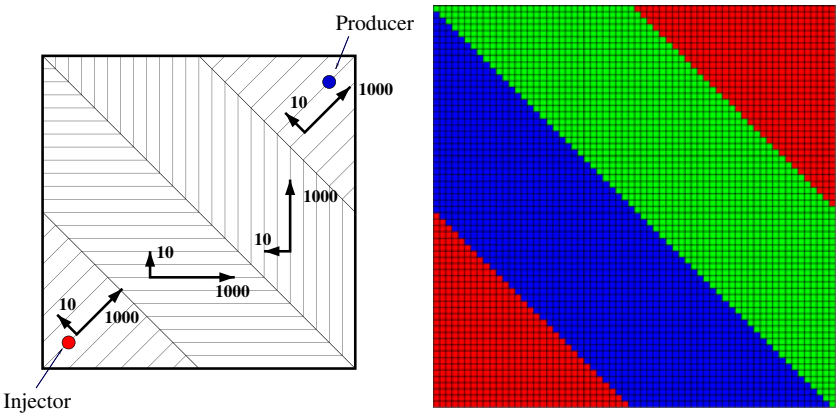

Fig. 8 *Left*: discontinuous anisotropic tensor. *Right*: sample mesh

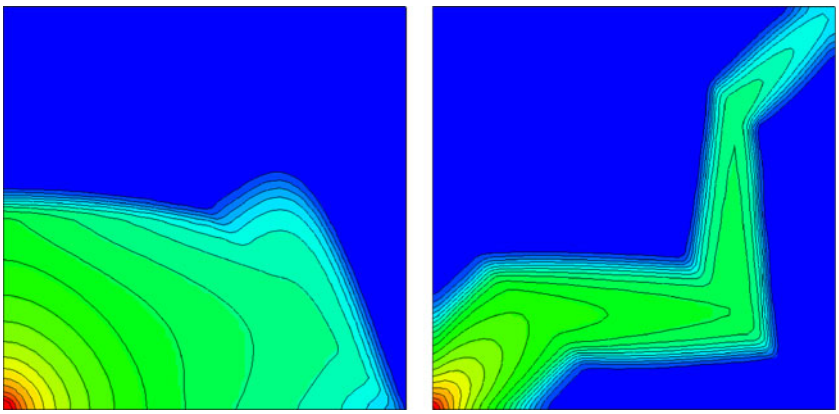

Fig. 9 Water saturation at $T = 55$ days. Discontinuous tensor with high anisotropy

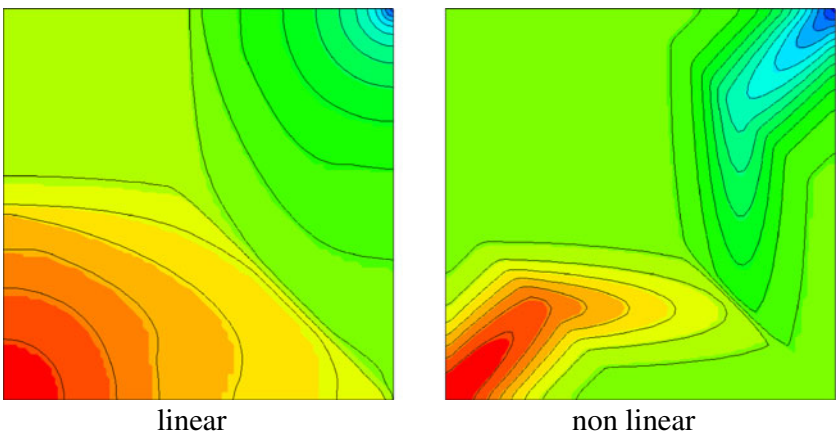

Fig. 10 Oil pressure at $T = 10$ days. Discontinuous tensor with high anisotropy

4.2 Discontinuous tensor with high anisotropy

In the next experiment, we use the uniform orthogonal $64 \times 64 \times 1$ grid M1, but with a discontinuous full anisotropic permeability tensor (see Fig. 8).

$$\mathbb{K} = R_z(-\theta)\ \ \mathrm{diag}(1{,}000,\ 10,\ 10)\ \ R_z(\theta),$$

where $\mathrm{diag}(k_1, k_2, k_3)$ is a diagonal matrix, $R_\alpha(\theta)$ is the rotation matrix in plane orthogonal to $o\alpha$ with angle θ.

The computational domain is 100 ft × 100 ft × 10 ft, and rotation angle is the following:

$$\theta = \begin{cases} 0^\circ & \text{if } 50\text{ ft} \le x + y < 100\text{ ft}, \\ 90^\circ & \text{if } 100\text{ ft} \le x + y < 150\text{ ft}, \\ 45^\circ & \text{if } x + y < 50\text{ ft, or } x + y \ge 150\text{ ft}. \end{cases}$$

Figure 9 shows the water saturation field at the moment $T = 55$ days and Fig. 10 presents the oil pressure field at the moment $T = 10$ days. The front propagations are completely different even if discretizations differ only near wells, where $\theta = 45^\circ$. Oil and water production rates are shown in Fig. 11.

4.3 Computational complexity

Different methods of flux approximation result in different computational work. The latter depends on sparsity of Jacobian matrix, convergence of Newton iterations, and convergence of the linear solver. We compare the linear TPFA, the nonlinear TPFA, and the conventional O-scheme for MPFA.

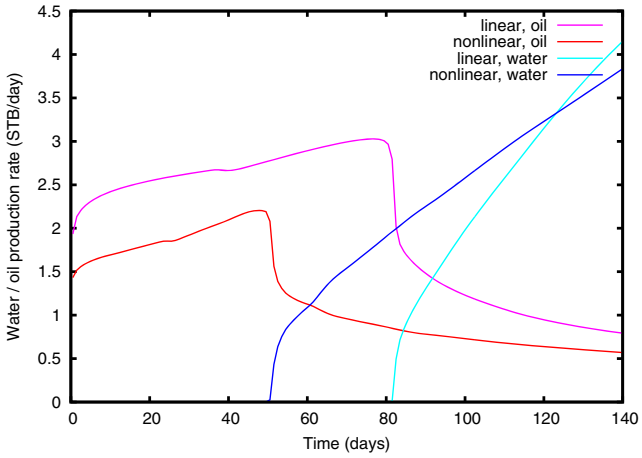

Fig. 11 Oil/water production rates. Discontinuous tensor with high anisotropy

We consider the simulation of water flooding process on slightly skewed nonorthogonal $32 \times 32 \times 8$ grid produced from the orthogonal grid by shifting grid nodes by $\Delta z = 0.01\,x + 0.02\,y$. Tensor $\mathbb{K}$ is the same as in the previous test case, $\theta = 30^\circ$.

Table 3 presents number of nonzero elements in Jacobian matrix, CPU time, total number of nonlinear and linear iterations for 200 days simulation using linear TPFA, nonlinear TPFA and MPFA methods. Boundary face unknowns are taken into account in the system in the simplest TPFA framework for all three discretization methods. The linear solver is ILU(1)-preconditioned BiCGStab iterations with termination threshold 10^{-12}, the Newton iterations terminate if the residual is less than 10^{-5}.

The nonlinear TPFA simulation is more expensive than the linear TPFA simulation due to less sparse Jacobian and greater number of accumulated BiCGStab iterations. On the other hand, our method is 2.4-fold faster than FV with MPFA. We should note that the linear TPFA provides wrong solution due to the lack of approximation on skewed meshes.

4.4 Monotonicity

In the last test case, we analyze the monotonicity quality of the new method and compare it with two convectional schemes.

We consider diffusion problem (1) defined in the unit cube with a cubic hole, $\Omega = (0, 1)^3/[0.4, 0.6]^3$. The boundary of Ω consists of two disjoint parts, interior Γ_0 and outer Γ_1. We set $\Gamma_N = \emptyset$, $f = 0$, $g_D = 2$ on Γ_0, $g_D = 0$ on Γ_1, and take the anisotropic diffusion tensor

$$\mathbb{K} = R_{xyz}\ \mathrm{diag}(300,\ 15,\ 1)\ R_{xyz}^T,$$

where $R_{xyz} = R_z(-\pi/6)R_y(-\pi/4)R_x(-\pi/3)$.

According to the maximum principle for elliptic PDEs, the exact solution should be between 0 and 2. Discrete solutions computed with the nonlinear TPFA on all types of the

Table 3 Total number of nonzero elements (nz) in Jacobian matrix, CPU time (seconds), total number of nonlinear (#nit.) and linear (#lit.) iterations for simulations with linear TPFA, nonlinear TPFA and MPFA schemes

Scheme	nz	Time		#nit	#lit
lin.TPFA	229 376	205.67 s	1.0x	653	15 896
nonl.TPFA	367 868	343.75 s	1.67x	664	23 924
MPFA	893 632	833.64 s	4.05x	660	26 288

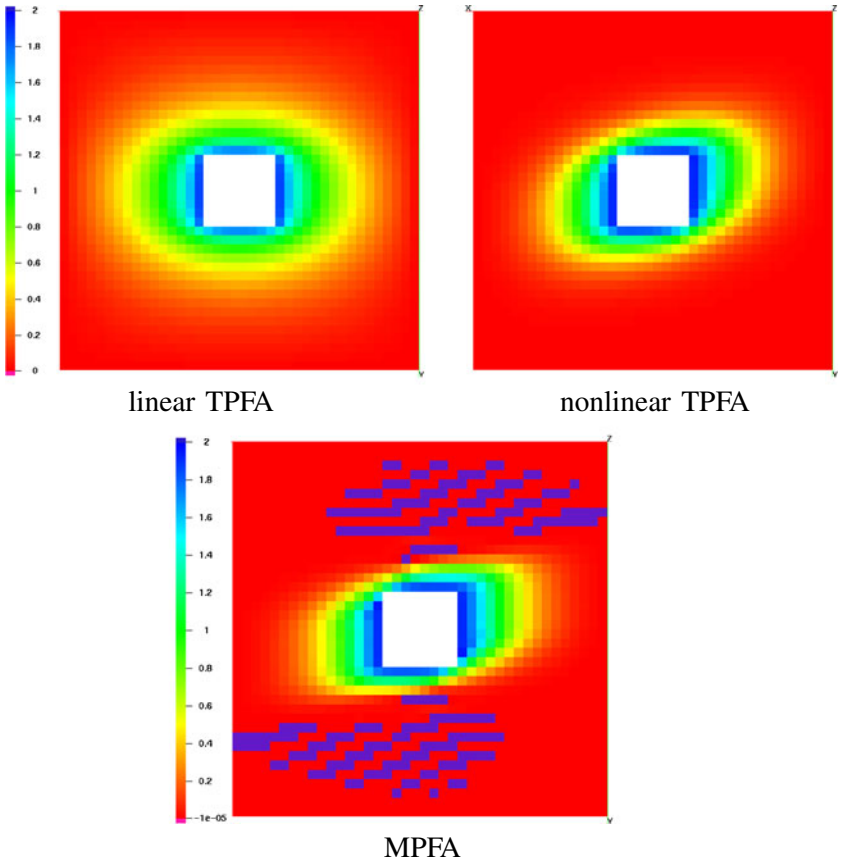

Fig. 12 Cutplane of the solution calculated with the linear TPFA, nonlinear TPFA, and MPFA FV methods for the problem with the Dirichlet boundary conditions. For MPFA scheme elements with solution values $< -10^{-5}$ are marked by different color. Orthogonal grid with $h = 1/40$

considered meshes (orthogonal or randomly distorted hexahedral, unstructured triangular prismatic, or tetrahedral) are nonnegative everywhere in Ω whereas the MPFA method produces large regions with negative concentrations even on orthogonal grid (see Fig. 12). We remark that MFE discretization also generates extensive areas of negative solution [5, 12, 13].

Table 4 presents the minimum and maximum values of the discrete concentration. The data show that both TPFAs give the discrete solution within [0, 2], and MPFA produces considerable undershoots and overshoots. The solution obtained by the linear TPFA is wrong due to the lack of approximation. Despite the fact that in this experiment the solution satisfies the DMP, one can find an example [5] where the principle is violated for nonlinear TPFA.

Table 4 Minimum and maximum concentration values for the problem with the Dirichlet boundary conditions (orthogonal grid with $h = 1/40$)

Scheme	$C_{\min}$	$C_{\max}$
lin.TPFA	1.3×10^{-5}	1.889
nonl. TPFA	1.6×10^{-10}	1.948
MPFA	-5.5×10^{-2}	2.087

5 Conclusions

We presented the new monotone cell-centered FV method. Its monotonicity is understood as nonnegative approximations of nonnegative solutions to partial differential equations. The method can be easily modified to provide the discrete maximum principle [15].

The cornerstone of the method is the nonlinear two-point flux approximation. Numerical experiments with the two-phase flow model demonstrate its superiority to the conventional linear TPFA and MPFA.

For $\mathbb{K}$-orthogonal grids, all considered discretizations are identical. However, in case of $\mathbb{K}$-nonorthogonal grids, the nonlinear TPFA provides more accurate and physically relevant front propagation and water breakthrough time than the conventional linear TPFA. The computational complexity of the new method for fully implicit time stepping scheme is greater than that of the linear TPFA and lesser than that of the MPFA (O-scheme). The linear TPFA may produce wrong solutions due to the lack of approximation.

References

1. Aavatsmark, I., Eigestad, G., Mallison, B., Nordbotten, J.: A compact multipoint flux approximation method with improved robustness. Numer. Methods Partial Diff. Equ. **24**(5), 1329–1360 (2008)
2. Aziz, K., Settari, A.: Petroleum Reservoir Simulation. Applied Science Publishers Ltd., London (1979)
3. Brezzi, F., Fortin, M.: Mixed and Hybrid Finite Element Methods. Springer-Verlag, New York (1991)
4. Chen, Z., Huan, G., Ma, Y.: Computational Methods for Multiphase Flows in Porous Media. SIAM (2006)
5. Danilov, A., Vassilevski, Y.: A monotone nonlinear finite volume method for diffusion equations on conformal polyhedral meshes. Russ. J. Numer. Anal. Math. Model. **24**(3), 207–227 (2009)
6. Kapyrin, I.: A family of monotone methods for the numerical solution of three-dimensional diffusion problems on unstructured tetrahedral meshes. Dokl. Math. **76**(2), 734–738 (2007)
7. Kuznetsov, Y., Repin, S.: New mixed finite elements method on polygonal and polyhedral meshes. Russ. J. Numer. Anal. Math. Model. **18**, 261–278 (2003)
8. LePotier, C.: Schéma volumes finis monotone pour des opérateurs de diffusion fortement anisotropes sur des maillages de triangle non structurés. C. R. Acad. Sci. Ser. I **341**, 787–792 (2005)
9. LePotier, C.: Finite volume Scheme Satisfying Maximum and Minimum Principles for Anisotropic Diffusion Operators, FVCA V. pp. 103–118 (2008)
10. LePotier, C.: Correction non linéaire et principe du maximum pour la discrétisation dopérateurs de diffusion avec des schémas volumes nis centrés sur les mailles. C. R. Acad. Sci. Ser. I **348**, 691–695 (2010)
11. Lipnikov, K., Gyrya, V.: High-order mimetic finite difference method for diffusion problem on polygonal meshes. J. Comp. Phys. **227**, 8841–8854 (2008)
12. Lipnikov, K., Svyatskiy, D., Shashkov, M., Vassilevski, Y.: Monotone finite volume schemes for diffusion equations on unstructured triangular and shape-regular polygonal meshes. J. Comp. Phys. **227**, 492–512 (2007)
13. Lipnikov, K., Svyatskiy, D., Vassilevski, Y.: Interpolation-free monotone finite volume method for diffusion equations on polygonal meshes. J. Comp. Phys. **228**(3), 703–716 (2009)
14. Lipnikov, K., Svyatskiy, D., Vassilevski, Y.: A monotone finite volume method for advection–diffusion equations on unstructured polygonal meshes. J. Comp. Phys. **229**, 4017–4032 (2010)
15. Lipnikov, K., Svyatskiy, D., Vassilevski, Y.: Minimal stencil finite volume scheme with the discrete maximum principle. Russ. J. Numer. Anal. Math. Model. **27**(4), 369–385 (2012)
16. Nikitin, K., Vassilevski, Y.: A monotone nonlinear finite volume method for advection–diffusion equations on unstructured polyhedral meshes in 3D. Russ. J. Numer. Anal. Math. Model. **25**(4), 335–358 (2010)
17. Nikitin, K.: Nonlinear finite volume method for two-phase flow in porous media (in Russian). Math. Model. **22**(11), 131–147 (2010)
18. Nikitin, K., Vassilevski, Y.: A Monotone Finite Volume Method for Advection Diffusion Equations and Multiphase Flows. In: Proceedings of the ECMOR XIII, EAGE (2012)
19. Peaceman, D.W.: Interpretation of Well-Block Pressures in Numerical Reservoir Simulation. SPEJ June, pp. 183–194 (1978)
20. Sheng, Z., Yuan, A.: Monotone finite volume schemes for diffusion equations on polygonal meshes. J. Comp. Phys. **227**(12), 6288–6312 (2008)
21. Sheng, Z., Yuan, A.: The finite volume scheme preserving extremum principle for diffusion equations on polygonal meshes. J. Comp. Phys. **230**(7), 2588–2604 (2011)
22. Terekhov, K., Vassilevski, Y.: Two-phase water flooding simulations on dynamic adaptive octree grids with two-point nonlinear fluxes. Russ. J. Numer. Anal. Math. Model. **28**(3) (2013). to appear
23. Vassilevski, Y., Kapyrin, I.: Two splitting schemes for nonstationary convection-diffusion problems on tetrahedral meshes. Comp. Math. Math. Phys. **48**(8), 1349–1366 (2008)